Applied Surface Science 257 (2011) 7900–7905

Contents lists available at ScienceDirect

Applied Surface Science

journal homepage: www.elsevier.com/locate/apsusc

Influence of annealing temperature on the structural, optical and mechanical properties of ALD-derived ZnO thin films

C.-Y. Yen [a], S.-R. Jian [a,*], G.-J. Chen [a], C.-M. Lin [b], H.-Y. Lee [c], W.-C. Ke [d], Y.-Y. Liao [e], P.-F. Yang [f], C.-T. Wang [f], Y.-S. Lai [f], Jason S.-C. Jang [g], J.-Y. Juang [h]

[a] Department of Materials Science and Engineering, I-Shou University, Kaohsiung 840, Taiwan
[b] Department of Applied Science, National Hsinchu University of Education, Hsinchu 300, Taiwan
[c] National Synchrotron Radiation Research Center, Hsinchu 300, Taiwan
[d] Department of Mechanical Engineering, Yuan Ze University, Tao-Tuan 32003, Taiwan
[e] Department of Applied Physics, National University of Kaohsiung, Kaohsiung 81148, Taiwan
[f] Central Product Solutions, Advanced Semiconductor Engineering, Inc., 26 Chin 3rd Rd., Nantze Export Processing Zone, Kaohsiung 811, Taiwan
[g] Department of Mechanical Engineering; Institute of Materials Science & Engineering, National Central University, Chung-Li 320, Taiwan
[h] Department of Electrophysics, National Chiao Tung University, Hsinchu 300, Taiwan

ARTICLE INFO

Article history:
Received 8 February 2011
Received in revised form 1 April 2011
Accepted 19 April 2011
Available online 27 April 2011

Keywords:
ZnO thin films
Atomic layer deposition
XRD
AFM
Nanoindentation
Hardness

ABSTRACT

ZnO thin films grown on Si(1 1 1) substrates by using atomic layer deposition (ALD) were annealed at the temperatures ranging from 300 to 500 °C. The X-ray diffraction (XRD) results show that the annealed ZnO thin films are highly (0 0 2)-oriented, indicating a well ordered microstructure. The film surface examined by the atomic force microscopy (AFM), however, indicated that the roughness increases with increasing annealing temperature. The photoluminescence (PL) spectrum showed that the intensity of UV emission was strongest for films annealed at 500 °C. The mechanical properties of the resultant ZnO thin films investigated by nanoindentation reveal that the hardness decreases from 9.2 GPa to 7.2 GPa for films annealed at 300 °C and 500 °C, respectively. On the other hand, the Young's modulus for the former is 168.6 GPa as compared to a value of 139.5 GPa for the latter. Moreover, the relationship between the hardness and film grain size appear to follow closely with the Hall–Petch equation.

1. Introduction

ZnO is a wide band gap semiconductor ($E_g \cong 3.4$ eV at room temperature) with high thermal and chemical stabilities. Moreover, the large exciton binding energy (~60 meV) for the pristine ZnO is more than twice larger than that obtained in GaN, making it one of the potential candidates for applications in blue and ultraviolet optical devices, such as light-emitting diodes and ultraviolet laser diodes [1–4]. However, depending on the fabricating methods and conditions, the photoluminescence investigations have revealed the intimated correlations between the specific emissions in the visible range and associated defects in ZnO films [5]. In addition to monitoring the electric and optical properties through careful control of the processing parameters, successful fabrication of devices based on the epitaxial ZnO thin films also requires better understanding of the mechanical characteristics, since the contact loading during processing or packaging can significantly degrade the performance of these devices. Therefore, there is a growing demand of investigating the mechanical characteristics of materials, in particular in the nanoscale regime. To this respect, nanoindentation has been serving as one of the powerful tools in unveiling important mechanical property parameters, such as the hardness and elastic modulus, of thin films [6–9] or small structures [10–12].

ZnO thin films can be deposited with a wide variety of methods, such as radio frequency magnetron sputtering [13], chemical vapor deposition (CVD) [14], molecular beam epitaxy (MBE) [15] and pulsed laser deposition [16]. Nevertheless, all of these methods require high processing temperatures to obtain decent electrical properties such as high mobility and low operation voltage for device applications, thus are not suitable for depositing ZnO films on flexible substrates or organic dielectrics. Recently, the atomic layer deposition (ALD) method has been successfully demonstrated its capabilities of depositing thin films at low temperatures. In particular, ALD offers good control in growing large area films with excellent thickness and composition uniformities. This study presents the nanomechanical characteristics and optical properties

* Corresponding author at: Department of Materials Science and Engineering, I-Shou University, Kaohsiung 840, Taiwan. Tel.: +886 7 6577711x3130; fax: +886 7 6578444.
E-mail address: srjian@gmail.com (S.-R. Jian).

0169-4332/$ – see front matter © 2011 Elsevier B.V. All rights reserved.
doi:10.1016/j.apsusc.2011.04.088

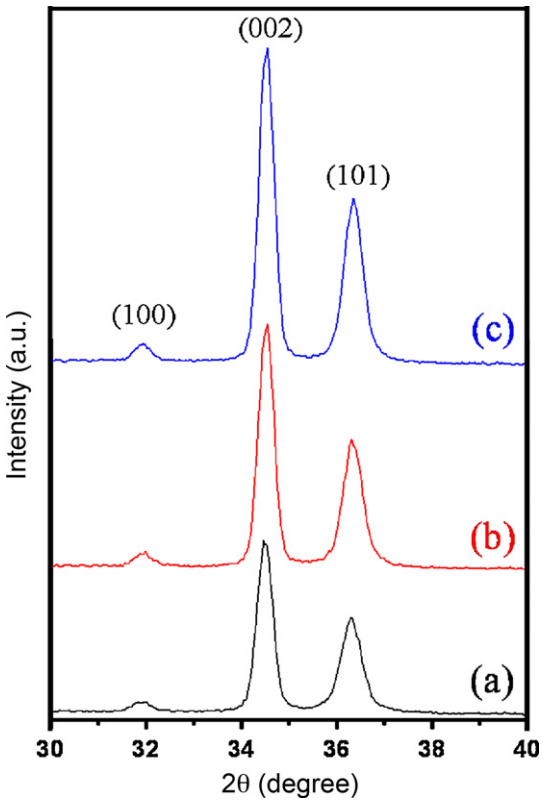

Fig. 1. XRD pattern of ZnO thin films annealed at (a) 300 °C, (b) 400 °C and (c) 500 °C.

of the ALD-derived ZnO thin films by using a Berkovich nanoindentation system operated in the continuous contact stiffness measurement (CSM) mode and photoluminescence (PL), respectively. Furthermore, the microstructure and surface morphology of the ZnO films were characterized by X-ray diffraction (XRD) and atomic force microscopy (AFM). The effects of annealing temperature on the optical and mechanical properties of ZnO films are discussed.

2. Experimental details

ZnO thin films were deposited on Si(1 1 1) substrates at room temperature by using an ALD system operated with flow-rate interruption method. The detailed growth procedures can be found elsewhere [17]. For a typical run of 1000 ALD cycles, the thickness of the as-deposited ZnO thin films was about 200 nm. Subsequently, the as-deposited ZnO thin films were post-annealed at the temperatures ranging from 300 °C to 500 °C for 1 h in atmosphere by rapid thermal annealing. The heating rate was set at 20 °C/s and it took about 30 min for the furnace to cool down to room temperature after annealing. The crystal structure of ZnO thin films were analyzed by XRD (X-ray diffraction, Panalytical X'Pert XRD). In addition, a Veeco/TM CP-R atomic force microscopy was used to examine the surface morphology of the samples. For the AFM operation, a constant scan speed of 1 μm/s was used, with a constant load of 30 nN being applied to the cantilever. The optical properties of the annealed ZnO thin films were investigated by PL measurements using a He–Cd laser of 325 nm with a power of 20 mW. A liquid–nitrogen cooled UV-enhanced CCD was used as detector placed behind a monochromator with 10 μm entrance slit for 0.02 nm spectrum resolution. PL measurement was performed at room temperature and the acquisition time was about 15 min.

Nanoindentation experiments were preformed on a MTS Nano Indenter® XP system with a three-sided pyramidal Berkovich indenter tip by using the CSM technique [18]. This technique is accomplished by imposing a small, sinusoidal varying force on top of the applied linear force that drives the motion of the indenter. The displacement response of the indenter at the excitation frequency and the phase angle between the force and displacement are measured continuously as a function of the penetration depth. Solving for the in-phase and out-of-phase portions of the displacement response gives rise to the determination of the contact stiffness as a continuous function of depth [18]. As such, the mechanical properties changing with respect to the indentation depth can be obtained. The nanoindentation measurements were carried out as follows. First, prior to applying loading on ZnO sample, nanoindentation was conducted on the standard fused silica sample to obtain the reasonable range (the Young's modulus of fused silica is 68–72 GPa). Then, a constant strain rate of 0.05 s^{-1} was maintained during the increment of load until the indenter reached 50 nm deep into the surface. The load was then held at the maximum value of loading for 10 s in order to avoid the creep, which might significantly affect the unloading behavior. The indenter was then withdrawn from the surface at the same rate until the loading has reduced to 10% of the maximum load. Then, the indenter was completely removed from the material. In this work, constant strain rate was chosen in order to avoid the strain-hardening effects. At least 30 indentations were performed on each sample and the distance between the adjacent indents was kept at least 50 μm apart to avoid interaction.

In indentation test, the hardness is defined as the applied indentation load divided by the projected contact area, as following:

$$H = \frac{P_{\max}}{A_c} \tag{1}$$

where A_c is the projected contact area between the indenter and the sample surface at the maximum indentation load, $P_{\max}$. For a perfectly sharp Berkovich indenter, projected area A_c can be calculated as, $A_c = 24.56h_c^2$ with h_c being the true contact depth.

The elastic modulus of the sample can be calculated based on the relationships developed by Sneddon [19]: $S = 2\beta E_r\sqrt{A_c}/\sqrt{\pi}$. Here S is the contact stiffness of the material, β is a geometric constant with $\beta = 1.00$ for Berkovich indenter, and E_r is the reduced elastic modulus which is calculated from the following equation:

$$\frac{1}{E_r} = \frac{1-\nu_f^2}{E_f} + \frac{1-\nu_i^2}{E_i} \tag{2}$$

Here ν is the Poisson's ratio and the subscripts i and f denote the parameters for the indenter and the annealed ZnO thin films, respectively. For diamond indenter tip, $E_i = 1141$ GPa, $\nu_i = 0.07$ and, $\nu_i = 0.25$ is chosen for ZnO thin films [17].

3. Results and discussion

3.1. Crystal structure and surface features

Fig. 1 shows part of the XRD results of the post-annealed ZnO thin films. The diffraction peaks from the Si(1 1 1) substrates, on which the films were grown, were not displayed in Fig. 1. The simultaneous appearance of all the three primary diffraction peaks, namely (1 0 0), (0 0 2), and (1 0 1) for all the annealed ZnO films indicates that all the films appear to crystallize equiaxially. In addition, it can be found that the intensity of (0 0 2) diffraction peak increases and the full width at half maximum (FWHM) becomes narrower with the increasing annealing temperature. The grain size, D, of the corresponding films can be estimated according to the Scherrer's equation [20]:

$$D = \frac{0.9\lambda}{B\ \cos\theta} \tag{3}$$

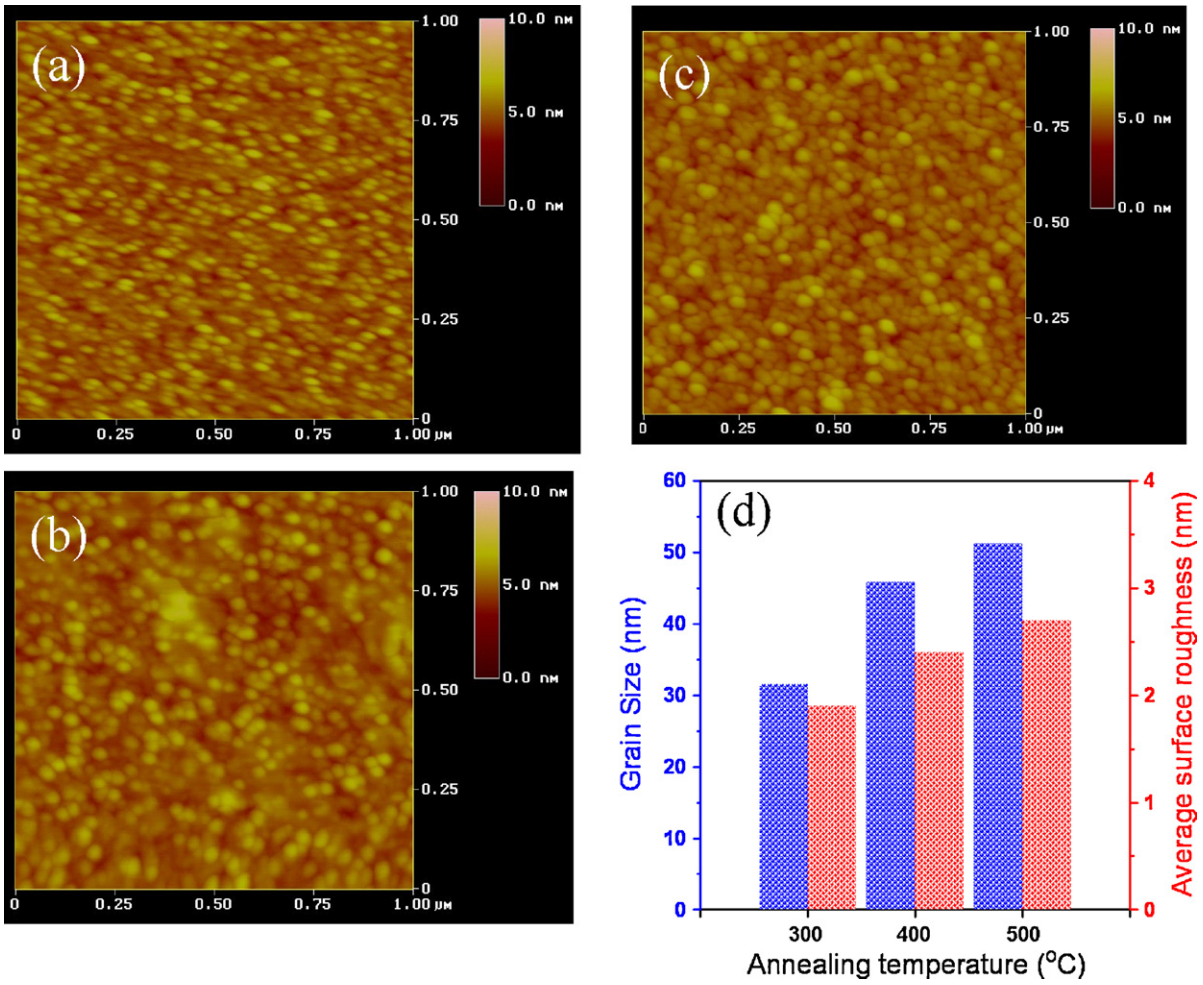

Fig. 2. Topography images for ZnO thin films annealed at (a) 300 °C, (b) 400 °C, (c) 500 °C measured by AFM and (d) annealed temperature dependence of the average surface roughness and grain size for ZnO thin films annealed at various temperatures.

where λ, B and θ are the X-ray wavelength, the FWHM of the ZnO (0 0 2)-oriented peak and Bragg diffraction angle, respectively. The estimated grain sizes for ZnO thin films annealed at 300, 400 and 500 °C are 31.5, 45.8 and 51.2 nm, respectively. As can be seen below, the AFM examinations on these films gave consistent results described above.

Fig. 2 shows the AFM images revealing the surface morphology of the annealed ZnO thin films. The root mean square roughness for ZnO thin films annealed at 300, 400, and 500 °C are 1.9, 2.4 and 2.7 nm, respectively. Furthermore, as shown in Fig. 2(a–c), the annealed ZnO thin films all exhibit similar dense microstructures with homogeneous grain sizes and the grain size appears to increase with increasing annealing temperature. The average grain size obtained from image analysis and displayed in the histogram shown in Fig. 2(d) indeed are consistent with the conjectures obtained from the XRD analyses. Namely, the microstructure of annealed ZnO films are equiaxed polycrystalline and the grain size increases from about 30 nm for thin films annealed at 300 °C to about 50 nm for thin films annealed at 500 °C. The grain growth of the ZnO thin films during annealing is presumably attributed to the enhanced diffusion of zinc and oxygen defects existing in the boundary. As sufficient thermal energy is provided by higher annealing temperature, it in turn facilitates the coalescence of the adjacent grains (or nuclei) and results in apparent grain growth [21]. The increase in film surface roughness (see also in the histogram shown in Fig. 2(d)) with increased annealing temperature can be considered also as a direct consequence of the surface diffusion enabled three-dimensional grain growth [22].

3.2. Optical characterizations

The room temperature PL characteristics of the annealed ZnO thin films, as displayed in Fig. 3, clearly shows that the primary emission is the near band edge emission centering around 380 nm. It is generally conceived that the UV emission peak originates from free excitonic recombination corresponding to the band edge emission of ZnO [23]. Therefore, the increased intensity of the UV emission band exhibited in Fig. 3, when the annealing temperature was increased from 300 °C to 500 °C, is indicative of significant improvement of crystalline quality resulted from the annealing. The present results are also in sharp contrast to ZnO films obtained by other methods, in that emission peaks in the visible bandwidths have been ubiquitously observed. This might be because that the ZnO thin films deposited by the low temperature ALD processes does not favor the formation of Zn–Zn bonds and forms primarily the Zn–O bonds, thus suppresses the emission in the wavelength region of visible light [24]. Alternatively, it can also be explained by the fact that the marked grain growth and associated recrystallization in the ZnO films induced by post-annealing might have

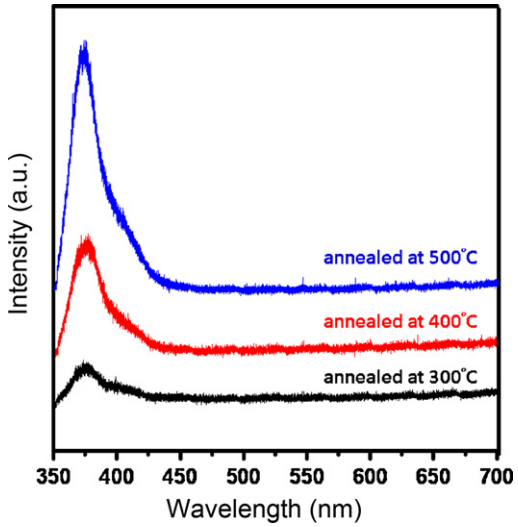

Fig. 3. Room temperature PL spectra of ZnO thin films annealed at temperature from 300 °C to 500 °C.

eliminated the majority of oxygen vacancies and other defects, which have been considered as the major sources of visible emissions observed in ZnO films [5]. We note that the results are also consistent with that obtained in the previous study [25]. In that the improvement in crystallinity of ZnO thin films due to annealing-induced increase in grain size and increasing dominance of certain crystal orientation was believed to have drastic effects in reducing the green emission and in increasing the UV emission.

3.3. Nanoindentation responses

Fig. 4(a) displays the typical load–displacement (P–h) curves reflecting the deformation history of ZnO thin film annealed at 300 °C during penetration of a Berkovich indenter loaded with CSM mode. The P–h response obtained by nanoindentation contains information about the elastic behavior and plastic deformation and, can be regarded as the "fingerprint" of the properties of ZnO thin films. In addition, the curve appears smooth and regular, without any discontinuities along either the loading or unloading segment, indicating that, unlike those observed in InP [26] and in Si [27], neither twinning nor pressure-induced phase transformation was involved in this case.

Fig. 4(b) presents the hardness and Young's modulus versus penetration depth curves for ZnO film annealed at 300 °C. The curves can be divided into two stages, namely, an initial increase to a maximum value followed by subsequent decrease to a constant value. The hardness is observed to increase with increasing penetration depth at small depth. The increase in hardness at small penetration depth is usually attributed to the transition between purely elastic to elastic/plastic contact. Only under the condition of a fully developed plastic zone does the mean contact pressure represent the hardness. When there is no plastic zone, or only a partially formed plastic zone, the mean contact pressure (which is measured using the Oliver and Pharr method) is usually smaller than the nominal hardness. After the first stage, the hardness decreases to constant stage and reaches a constant value, which is consistent with the fact that a single material is being measured. The hardness values obtained at this stage, thus, can be regarded as intrinsic properties of the films. The penetration depth dependence of the Young's modulus, as illustrated in Fig. 4(b), behaves similarly as that of hardness. Consequently, both mechanical parameters were determined by taking the average values obtained by the CSM loading scheme (Fig. 4(b)) within the penetration depth of 20–50 nm. This range of

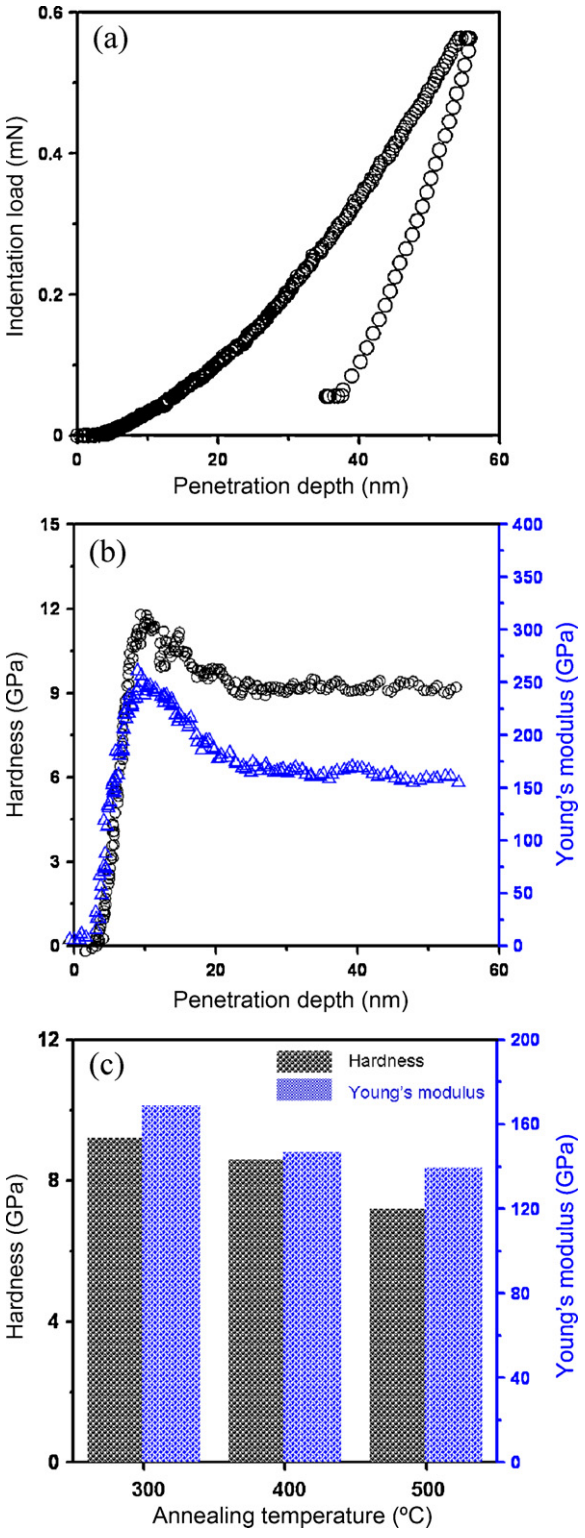

Fig. 4. Nanoindentation results: (a) a typical load–displacement curve and (b) the hardness and Young's modulus vs. displacement curves of annealed ZnO thin film at 300 °C, (c) hardness and Young's modulus of ZnO thin films annealed at various temperatures.

penetration depth was chosen intentionally to be deep enough for observing plastic deformation during indentation yet to be shallow enough to avoid the complications arising from the effects of surface roughness [28] and substrate [29].

Fig. 4(c) shows the hardness and Young's modulus obtained from ZnO thin films annealed at the different temperatures. It is

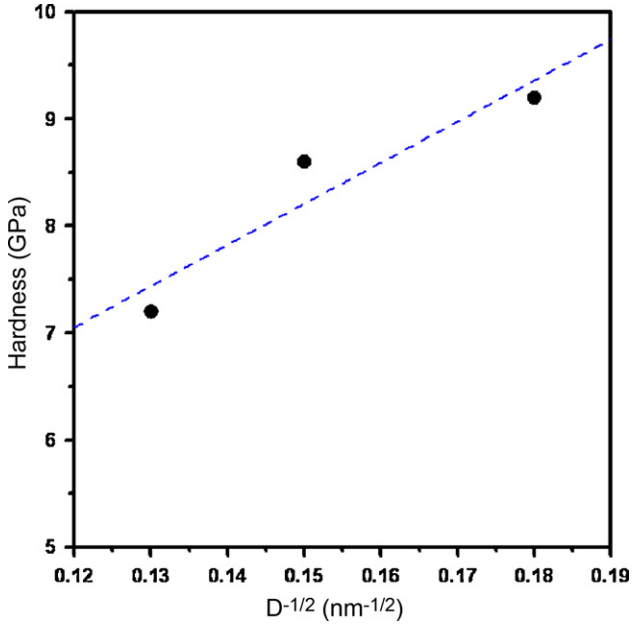

Fig. 5. Plot of the experimental data of hardness versus grain size. The dashed line represents a fit to the Hall–Petch equation with $H(D) = 2.44 + 38.4D^{-1/2}$.

evident that both the hardness and the Young's modulus of the ZnO films decrease monotonically with increasing annealing temperature. The corresponding hardness (Young's modulus) are 9.2 (168.6), 8.6 (145.4) and 7.2 (139.5) GPa for ZnO films annealed at 300 °C, 400 °C and 500 °C, respectively. Since the higher annealing temperature leads to the larger grain size for ZnO thin films, as we have discussed previously, it is reasonable to consider that the decrease of hardness and the Young's modulus might be mainly due to the grain size effect [30].

It is well known that the dependence of material hardness on the grain size can be described by the phenomenological "Hall–Petch" equation [31]:

$$H(D) = H_0 + k_{H-P}D^{-1/2} \quad (4)$$

where H_0 and k_{H-P} denote the lattice friction stress and the Hall–Petch constant, respectively. Fig. 5 displays a plot of the hardness versus $D^{-1/2}$ data for ZnO thin films annealed at various temperatures. We note that although the grain size of annealed ZnO thin films remains relatively small as compared to that of the usual metallic materials, the data still follow pretty closely to the Hall–Petch relation and the so-called negative Hall–Petch effect [32] is not observed here. The dashed line represents the fit to the Hall–Petch equation for the experimental data, which gives:

$$H(D) = 2.44 + 38.4D^{-1/2} \quad (5)$$

The obtained lattice friction stress of 2.44 GPa is consistent with the reported bulk values where the hardness values measured along the *a*-axis and *c*-axis hardness were 2 ± 0.2 and 4.8 ± 0.2 GPa, respectively [33]. The Hall–Petch constant of 38.4 GPa $nm^{1/2}$ for the annealed ZnO films also indicates the effectiveness of the grain boundary in hindering the dislocation movements. In any case, both of the optical and mechanical properties obtained in the present study indicate that the intrinsic properties of the ZnO are closely reproduced in these post-annealed ALD-derived ZnO films.

4. Conclusion

In this study, we have carried out XRD, AFM, PL, and nanoindentation measurements to examine systematically the effects of post-annealing on the structural features, optical and mechanical characteristics of ZnO thin films deposited on Si(1 1 1) substrates by atomic layer deposition process. The main findings are summarized as following:

(1) The XRD results and the atomic force microscopy consistently and quantitatively indicated that the increases of both of the grain size and surface roughness with increased annealed temperatures might have been due primarily to the surface diffusion dominated three-dimensional grain growth mechanism.
(2) The PL characteristics showed significant enhancement in the intrinsic band edge UV emission when ZnO films were subjected to annealing treatment. The correlation of the intensity of the UV emission peak with the annealing temperature, and hence the improving crystallinity of the ZnO films and, the absence of emissions in the visible range for the annealed ZnO films suggested the marked effects of annealing in removing the defects introduced during the deposition processes from the ZnO films.
(3) The hardness and Young's modulus of the ZnO films were determined by the nanoindentation measurements. In addition, it has been demonstrated that the hardness of the ZnO films follows satisfactorily with the Hall–Petch equation, and the obtained lattice friction stress of 2.44 GPa is consistent with the bulk values obtained from single crystalline ZnO. The Hall–Petch constant of 38.4 GPa nm1/2 suggests the effectiveness of grain boundary in inhibiting the dislocation movement in ZnO.

Acknowledgements

This work was partially supported by the National Science Council of Taiwan, under grant no.: NSC97-2112-M-214-002-MY2 and NSC99-2112-M-214-001. JYJ is partially supported by the MOE-ATU program operated at NCTU.

References

[1] A.P. Alivisato, Science 271 (1996) 933.
[2] K.C. Aw, Z. Tsakadze, A. Lohani, S. Mhaisalkar, Scripta Mater. 60 (2009) 48.
[3] T. Makino, C.H. Chia, T.T. Nguen, Y. Segawa, Appl. Phys. Lett. 77 (2000) 1632.
[4] Y. Ryu, T.S. Lee, J.A. Lubguban, H.W. White, B.J. Kim, Y.S. Park, Appl. Phys. Lett. 88 (2006) 241108.
[5] Y.M. Chang, S.R. Jian, H.Y. Lee, C.M. Lin, J.Y. Juang, Nanotechnology 21 (2010) 385705.
[6] C.H. Chien, S.R. Jian, C.T. Wang, J.Y. Juang, J.C. Huang, Y.S. Lai, J. Phys. D: Appl. Phys. 40 (2007) 3985.
[7] S.R. Jian, J.Y. Juang, Y.S. Lai, J. Appl. Phys. 103 (2008) 033503.
[8] S.R. Jian, G.J. Chen, T.C. Lin, Nanoscale Res. Lett. 5 (2010) 935.
[9] S.R. Jian, J.Y. Juang, N.C. Chen, S.C. Jason, J.C. Jang, Y.S. Huang, Lai, Nanosci. Nanotechnol. Lett. 2 (2010) 315.
[10] X. Tao, X.D. Li, Nano Lett. 8 (1008) 505.
[11] L. Bao, Z.H. Xu, R. Li, X.D. Li, Nano Lett. 10 (1008) 255.
[12] T.H. Sung, J.C. Huang, J.H. Hsu, S.R. Jian, Appl. Phys. Lett. 97 (2010) 171904.
[13] P.F. Yang, H.C. Wen, S.R. Jian, Y.S. Lai, S. Wu, R.S. Chen, Microelectron. Reliab. 48 (2008) 389.
[14] Q.W. Li, J.M. Bian, J.C. Sun, H.W. Liang, C.W. Zou, Y.L. Sun, Y.M. Luo, Appl. Surf. Sci. 257 (2010) 1634.
[15] X.Q. Wang, H.P. Sun, X.Q. Pan, Appl. Phys. Lett. 97 (2010) 151908.
[16] S.R. Jian, I.J. Teng, P.F. Yang, Y.S. Lai, J.M. Lu, J.G. Chang, S.P. Ju, Nanoscale Res. Lett. 3 (2008) 186.
[17] C.S. Ku, J.M. Huang, C.M. Lin, H.Y. Lee, Thin Solid Films 518 (2009) 1373.
[18] X.D. Li, B. Bhushan, Mater. Charact. 48 (2002) 11.
[19] I.N. Sneddon, Int. J. Eng. Sci. 3 (1965) 47.
[20] B.D. Cullity, S.R. Stock, Element of X-ray diffraction, Prentice Hall, New Jersey, 2001, p170.
[21] E. Cetinorgu, S. Goldmith, R.L. Boxman, Surf. Coat. Technol. 201 (2007) 7266.
[22] Z.B. Fang, Z.J. Yan, Y.S. Tan, X.Q. Liu, Y.Y. Wang, Appl. Surf. Sci. 241 (2005) 303.
[23] Y. Chen, D.M. Bagnall, H.J. Koh, K.T. Park, K. Hiraga, Z.Q. Zhu, T. Yao, J. Appl. Phys. 84 (1998) 3912.
[24] J. Lim, K. Shin, H.W. Kim, C. Lee, J. Lumin. 109 (2004) 181.
[25] J. Zhao, L. Hu, Z. Wang, Y. Zhao, X. Liang, M. Wang, Appl. Surf. Sci. 229 (2004) 311.
[26] S.R. Jian, S.C. Jason, Jang, J. Alloys Compd. 482 (2009) 498.

[27] S.R. Jian, G.J. Chen, J.Y. Juang, Curr. Opin. Solid State Mater. Sci. 14 (2010) 69.
[28] M.S. Bobji, S.K. Biswas, J.B. Pethica, Appl. Phys. Lett. 71 (1997) 1059.
[29] X.D. Li, H. Gao, C.J. Murphy, K.K. Caswell, Nano Lett. 11 (2003) 1495.
[30] P. Delobelle, O. Guillon, E. Fribourg-Blanc, C. Soyer, E. Cattan, D. Rèminens, Appl. Phys. Lett. 85 (2004) 5185.
[31] S. Zhang, D. Sun, Y.Q. Fu, H.J. Du, Surf. Coat. Technol. 167 (2003) 113.
[32] H. Conrad, J. Narayan, Scripta Mater. 42 (2000) 1025.
[33] V.A. Coleman, J.E. Bradby, C. Jagadish, P. Munroe, Y.W. Heo, S.J. Pearton, D.P. Norton, M. Inoue, M. Yano, Appl. Phys. Lett. 86 (2005) 203105.